Interleukin-17 drives sex-dependent weight loss and changes in feeding behaviour during *Trypanosoma brucei* infection

Matthew C. Sinton[1,2¶*], Alex Girard[1,2], John Ogunsola[1,2], Praveena Chandrasegaran[1,2], Paul Capewell[1,2], Georgia Perona-Wright[1,3], Dieudonné M. Ngoyi[4,5], Nono Kuispond[4,5], Bruno Bucheton[5,6], Mamadou Camara[5,7], Shingo Kajimura[8,9], Cécile Bénézech[10], Annette MacLeod[1,2,5¶], Juan F. Quintana[1,2¶*]

[1]Wellcome Centre for Integrative Parasitology, University of Glasgow, Glasgow, UK. [2]School of Biodiversity, One Health and Veterinary Medicine, University of Glasgow, Glasgow, UK. [3]School of Infection and Immunity, University of Glasgow, Glasgow, UK. [4]Department of Parasitology, National Institute of Biomedical Research, Kinshasa, Democratic Republic of Congo. [5]Member of TrypanoGEN. [6]Institut de Recherche pour le Développement, Unité Mixte de Recherche IRD-CIRAD 177, Campus International de Baillarguet, Montpellier, France. [7]Programme National de Lutte contre la Trypanosomiase Humaine Africaine, Ministère de la Santé, Conakry, Guinea. [8]Division of Endocrinology, Diabetes and Metabolism, Beth Israel Deaconess Medical Center and Harvard Medical School, Boston, Massachusetts, USA. [9]Howard Hughes Medical Institute, Chevy Chase, Maryland, USA. [10]Centre for Cardiovascular Science, University of Edinburgh, Edinburgh, EH16 4TJ, Scotland, UK

[¶]These authors contributed equally to this work

*Corresponding authors

Email: matthew.sinton@glasgow.ac.uk (MCS), juan.quintana@glasgow.ac.uk (JFQ)

Abstract

Previous work has demonstrated that *Trypanosoma brucei* occupy several adipose tissue depots, including the subcutaneous adipose tissue in mice and humans, and due to its proximity to the skin, it is proposed to be an important for transmission. Here, we demonstrate that parasites in the inguinal white adipose tissue (iWAT) niche induce sexually dimorphic responses. During infection, male mice experience reduced adipose tissue mass, altered tissue function, and changes in feeding behaviour, whereas females do not. This tissue impairment correlates with an accumulation of T_H17 T cells in the iWAT. Genetic ablation of IL-17A/F abolishes infection-associated weight loss and alters feeding behaviour, limiting tissue wasting in male mice. Importantly, we detected a significant elevation in serum IL-17A in sleeping sickness patients, indicating that IL-17A/F signalling is also conserved in humans. We propose a model whereby IL-17A/F acts locally in adipocytes *via* engagement with its cognate receptor leading to lipolysis and tissue wasting, and/or systemically, *via* signalling in the hypothalamus to modulate feeding behaviour. Together, our findings suggest key sex-dependent roles for IL-17A/F in regulating adipose tissue and energy balance, as well as a coordinator of brain-adipose tissue communication during sleeping sickness, opening new directions to understand energy balance during infection.

Introduction

Trypanosoma brucei is an extracellular protozoan parasite that infects humans and livestock, causing Human African Trypanosomiasis (HAT, or sleeping sickness) and Animal African Trypanosomiasis (AAT, or nagana), respectively (Kennedy, 2019). Both HAT and AAT are prevalent in sub-Saharan regions of the African continent, where they impose a significant socio-economic burden, and are fatal if left untreated (Bukachi et al., 2017). Chronic infections in both humans and non-primate mammalian hosts, such as domestic cattle, lead to significant weight loss, a phenomenon that remains largely unstudied (Kennedy, 2013).

Upon infection, trypanosomes proliferate and migrate into tissues throughout the body, where they persist and form extravascular reservoirs in virtually every organ (Malvy and Chappuis, 2011). One major consequence of infection is weight loss, typically coupled with a reduction in adipose tissue mass, referred to as “tissue wasting” (Baazim et al., 2022). Previous studies have elegantly shown that male mice lose weight during *T. brucei* infection and that this is associated with wasting of the gonadal white adipose tissue (gWAT) (Trindade et al., 2016). Indeed, during the course of infection, *T. brucei* forms a reservoir in the gWAT, leading to an expansion of immune cells within the tissue, including macrophages, neutrophils, T helper (T_H)1 cells, effector $CD8^+$ cytotoxic T cells, and B cells (Hube and Hauner, 1999; Machado et al., 2021; Zúñiga et al., 2010), suggesting that adipose tissue wasting might be driven by the parasites, the immune response against them, or both.

Adipose tissue is also influenced by immune-derived factors under normal physiological conditions; For example, tumour necrosis factor (TNF) and interleukin-17A (IL-17A) have been shown to regulate adipose tissue structure and function, limiting tissue expansion (Hube and Hauner, 1999), and promoting adipogenesis (Zúñiga et al., 2010), respectively. Furthermore, IL-17A, and signalling through the IL-17C receptor, have been shown to induce thermogenesis in white and brown adipose tissue, respectively (Hu et al., 2020; Kohlgruber et al., 2018), and activation of thermogenesis, following challenges such as cold exposure, leads to increased energy expenditure (van Marken Lichtenbelt and Schrauwen, 2011). IL-17 has also been shown to play a role in controlling resistance to *T.*

cruzi infection (Guedes et al., 2010), which also leads to weight loss in humans (Cabalén et al., 2016). Furthermore, IL-17 was demonstrated to improve control of parasitaemia in female mice during infection with *T. congloense* (Mou et al., 2010), the parasite responsible for causing AAT. However, it remains unclear how the immune response to *T. brucei* infection influences adipose tissue structure and function.

Previous studies from our lab identified the skin as another reservoir for *T. brucei* and highlighted the presence of parasites in the adjacent subcutaneous white adipose tissue (scWAT) of infected patients (Capewell et al., 2016). Due to its proximity to the skin, we focused on understanding the impact of infection on the structure and function of the inguinal white adipose tissue (iWAT) in mice, which is traditionally used to model scWAT in humans (Chusyd et al., 2016). Like gWAT, the iWAT acts as an energy reservoir under homeostatic conditions and modulates systemic metabolism and appetite (Choe et al., 2016) . During times of nutrient deficiency, such as during food deprivation, iWAT increases lipolysis to release nutrients to maintain homeostasis of the organism, leading to tissue remodelling and size reduction (Finn and Dice, 2006). Infection also places a high energy demand on the host, due to activation of the immune response, and if this demand is not met through the intake of nutrients, then the host will use endogenous energy stores such as the adipose tissue, leading to wasting (Childs et al., 2019). Intriguingly, despite the energetic requirements of the immune response, sickness-induced anorexia is a central feature of infection-induced sickness behaviour (Adelman and Martin, 2009). Whilst this paradoxical behaviour is not yet fully understood, there are indications that it is related to cytokine signalling in the hypothalamus (Aviello et al., 2021).

Here we present data demonstrating that *T. brucei* infection is associated with sexually dimorphic immune responses in the adipose tissue and provide evidence that IL-17A/F influences adipose tissue wasting and feeding behaviour. These results provide novel insights into the role of IL-17A/F as a regulator of adipose tissue structure and function and feeding behaviour during infection. Furthermore, these findings support the utility of *T. brucei* infection

models for interrogating the role that IL-17A/F plays in controlling energy balance in other diseases.

Results

Infection with *T. brucei* leads to weight loss in a sex-dependent manner

In both humans and livestock, trypanosome infections are known to cause weight loss, and this has been recapitulated in male mouse models of infection (Trindade et al., 2016). However, direct comparisons have not been made between male and female mice to assess whether infection induces weight loss in a sexually dimorphic manner. To test this, we infected age-matched male and female C57BL/6 mice for a period of 25 days. We first wanted to determine that mice were successfully infected and whether there were differences between the levels of circulating parasites between sexes. Parasitaemia measurements followed a characteristic pattern, with no significant differences between sexes (**Figure 1A**). There were also no significant differences in the clinical scores of the mice (**Figure 1B**). Strikingly, during the course of infection, infected male mice lost significant amounts of bodyweight, whereas there was no significant difference between the weights of naïve and infected female mice (**Figure 1C** and **Figure 1D**). Spleen mass increased similarly in both male and female mice (**Supplementary Figure 1**), suggesting that changes in spleen mass during infection do not explain the differences in males and females.

Weight loss may be explained as a consequence of adipose tissue wasting (Dahlman et al., 2010), as a consequence of changes in feeding behaviour (Aviello et al., 2021), or both. To understand this in more detail, we measured gross food intake as a proxy for feeding behaviour. Over the course of infection, the food intake of infected male mice decreased from the onset of infection until 11 days post-infection (dpi), after which it increased to that of naïve males, before dropping again at 25 dpi (**Figure 1E**). Infected female mice displayed a brief, but non-significant, reduction in food intake at 7 dpi, but otherwise maintained a similar feeding behaviour profile to their wild type counterparts (**Figure 1F**). Taken together, these data suggests that weight loss during experimental trypanosomiasis occurs in a sex-dependent manner and is coupled, in males, to feeding behaviour.

T. brucei infection reduces iWAT mass and impairs tissue function

We next explored the impact of *T. brucei* infection on the adipose tissue. In addition to changes in feeding behaviour (Aviello et al., 2021), weight loss is typically associated with reductions in adipose tissue mass (Sun et al., 2020). We were particularly interested in the inguinal white adipose tissue (iWAT), which is analogous to the subcutaneous white adipose tissue beneath the skin in humans, as this constitutes an important parasite niche for disease transmission, especially in asymptomatic carriers (Capewell et al., 2016). In a seminal study, Trindade *et al* (2016) identified that colonisation of the gonadal white adipose tissue (gWAT) is associated with weight loss and reduction in adipose mass (Trindade et al., 2016), but the effect on iWAT, which is distinct from gWAT (**Figure 2A**), was not investigated. We first determined the presence of parasites in the iWAT and gWAT by histological analysis (**Figure 2B**) and, as expected, detected trypanosomes in both tissues. Next, we quantified trypanosome genomic DNA in the iWAT and gWAT as a proxy for determining parasite density, as previously performed (Machado et al., 2021). This highlighted that in male mice there were fewer parasites in the iWAT compared with the gWAT, but that there were no differences between these depots in females (**Figure 2C**). Together, these data suggest that African trypanosomes also establish infectious niches in the iWAT, proximal to the skin.

Following our observations of weight loss and the presence of trypanosomes in the iWAT, we then proceeded to characterise the impact of infection on this adipose tissue depot. When normalised to bodyweight, we found that infection led to a significant reduction in the adipose tissue mass of male mice (**Figure 2D**). Female mice also experienced some reduction in iWAT mass, but this was not significant. This raised the question of whether the reduction in mass is due to a loss of lipid content and reduction in adipocyte size (hypotrophy). To address this, we performed Haematoxylin and Eosin (H&E) staining of iWAT at 25 dpi. Visual assessment of the staining indicated that the iWAT of mice infected with *T. brucei* undergoes hypotrophy, with concurrent infiltration of immune cells (**Figure 2E**). To quantify lipid droplet size, which is a proxy for their lipid content, we used the software Adiposoft (Galarraga et al., 2012), Notably, in naïve animals, the size of lipid droplets was almost indistinguishable

between males and females, with lipid droplet area ranging from 50 to 700 μm^2 (**Figure 2F**). In contrast, the size range distribution between infected males and females was more constrained, ranging from 50-100 μm^2 (males) up to 300 μm^2 (females) (**Figure 2G**).

Considering the extensive wasting of this tissue, we questioned whether this impacted adipose tissue function. We measured blood glycerol levels as a broad marker of tissue function, as it reflects adipose tissue lipolysis rates throughout the body (Duncan et al., 2007). In both infected male and female mice, the circulating glycerol levels were significantly reduced (**Figure 2H**), although there were no sex-specific differences. The changes in glycerol levels observed in experimental infections were also replicated in the serum of stage II HAT patients from the towns of Boffa, Forécariah and Dubréka in Guinea, suggesting that the adipose tissue dysfunction induced by infection also occurs in humans (**Figure 2I**). Taken together, these findings highlight that *T. brucei* infection is associated with significant iWAT wasting and that this, in turn, is associated with impaired tissue function in both mice and humans. Thus, iWAT wasting could influence systemic metabolism, which, in turn, which may ultimately impact immune cell function.

Colonisation of iWAT by *T. brucei* is characterised by upregulation of CD4$^+$ T$_H$17 T cell related transcripts in males but not in females

To better understand the iWAT response to infection, and to identify potential drivers of tissue wasting, we performed bulk transcriptomics analysis of iWAT harvested at 25 dpi from both sexes and included naïve controls for comparison. Principal component analysis (PCA) revealed high levels of variance between naïve and infected males, but less variance between naïve and infected females (**Figure 3A**), potentially indicating a higher transcriptional response in the iWAT of male mice compared to female mice. Indeed, differential expression analysis revealed upregulation of 2,474 genes with a $\log_2$Fold change >0.5 and an adjusted *p* value of <0.05 that were common to both males and females, in addition to 1,410 male- and 668 female-specific gene signatures (**Figure 3B**). Of the 2,474 most of the significantly dysregulated genes (*padj* < 0.01) in both males and female mice, we detected robust

transcriptional signatures associated with recruitment and activation of the immune system (**Figure 3C**; e.g. *Lyz2, Slamf8, Aif1, Calhm6, Gzmb, Klra2,* and *Clec12a*).

Based on the observed adipose tissue wasting, we hypothesised that adipocyte hypotrophy is driven by increased rates of fatty acid oxidation and overall upregulation of energy metabolism. However, using pathway enrichment analysis, we found extensive downregulation of genes related to mitochondrial carbon (including *Idh1*, *Sdha*, *Mdh1*, and subunits of NADH:ubiquinone oxidoreductase and ATPase) and lipid metabolism and storage (including *Pnpla2*, *Cpt2*, *Plin1*, *Plin4*, and *Plin5*) (**Supplementary Table 1**). When we performed pathway enrichment analyses on upregulated genes, we identified common gene signatures in both males and females, including genes related to host response to parasitic and viral infections (leishmaniasis and SARS-CoV-2), including *Ifng*, *Il1b Tlr4*, and *Nlrp3* (**Supplementary Table 2**).

Next, we sought to understand which gene pathways are discriminatory between male and female mice. Pathway enrichment analysis of genes exclusively upregulated in females highlighted genes related to folate metabolism (including *Mocs1*, *Mocos*, and *Dhfr*), and protein processing in the endoplasmic reticulum (including *Ero1*, *Pdia4*, and *Pdia6*) (**Supplementary Table 2**). In contrast, several immune-related pathways were exclusively upregulated in males during infection, including those related to T cell signalling and T helper (T_H) cell differentiation: T_H1, T_H2, and T_H17 cells (**Supplementary Table 2**). Upregulated T_H1- and T_H2-related transcripts included *Nfatc1*, *Cd4*, *Cd3e*, *Runx3,* and *Gata3*, suggesting that T_H1 cells may be a significant contributor to interferon gamma ($IFN\gamma$) production during infection in the adipose tissue. Additionally, we also detected a significant upregulation of genes typically associated with differentiation of T_H17 effector cells, including *Irf4*, *Cd4*, *Cd3e*, *Il21r*, and *Il6ra* (**Figure 3D**). Taken together, we conclude that the iWAT of male mice experiences a robust pro-inflammatory response potentially mediated by T_H1 and T_H17 effector T cells, whereas the iWAT of infected female mice display transcriptional signatures associated with metabolism and protein synthesis.

T_H17 effector T cells accumulate in the adipose tissue during chronic *T. brucei* infection

Based on these observations, we hypothesised that T_H17 cells are important for the adipose immune response to infection. To quantify the different populations of $CD4^+$ T cells, including T_H17 cells, present in the iWAT during chronic *T. brucei* infection, we utilised mass cytometry by time of flight (CyTOF), enabling us to gain as much information as possible from the wasted adipose tissue. Previous studies, exploring the gWAT described an expansion of B cells, macrophages, granulocytes, and T cells (Machado et al., 2021). Using a broad panel, we also measured these immune populations in the iWAT (**Figure 4A**). Strikingly, $CD19^+$ B cells in the iWAT represent a smaller proportion of immune cells in males during infection, compared with naïve animals (**Figure 4B**). In contrast, in females, the proportion of iWAT $CD19^+$ B cells remains unaltered during infection, suggesting that B cell expansion in adipose tissue is both depot and sex specific. In both males and females, we observed expansion of macrophages and granulocytes (**Figure 4C** and **4D**, respectively), consistent with previous studies of gWAT in male mice (Machado et al., 2021). We further observed expansion of dendritic cells in both male and female mice during infection, but this was more pronounced in males (**Figure 4E**). Taken together, this suggests that immune population dynamics in the iWAT are sex specific.

Regarding the T cell effector population, we observed an increase in the proportion of $CD3\varepsilon^+$ $TCR\beta^+$ $CD4^+$ T cells in the iWAT of infected mice (**Figure 4F**) and, in particular, we identified an expansion of T effector (Teff) cells ($CD44^+$ and $CD69^+$) (**Figure 4G**). Whilst the frequency of $CD4^+$ T cells increased in both males and females, the iWAT of infected females contained a higher proportion of Teff cells compared with males. The expanded Teff cells displayed an elevated production of interferon gamma (IFNγ; **Figure 4H**), suggesting that some of these cells are polarised towards a T_H1 phenotype. Furthermore, there was a significant expansion of IL-17A-producing Teff cells (**Figure 4I**), indicating that cells are also polarised to a T_H17 phenotype and are a source of IL-17A. In contrast to our hypothesis, we observed a similar expansion of IL-17A-producing Teff cells in both infected males and females. However, we did observe that expression of the IL-17A receptor (*Il17ra*) is

significantly elevated in the iWAT of infected male mice, but not females (**Figure 4J**), suggesting that the adipose tissue of males becomes more responsive to IL-17A signalling during infection. Furthermore, IL-17A was elevated in the serum of infected males and female mice, as well as other inflammatory cytokines such as TNFα and IFNγ, compared to naïve controls (**Figure 4K**, **4L** and **4M**, respectively), consistent with previous reports (Magez et al., 1999; Wu et al., 2017). Moreover, we also detected a significant increase in the levels of circulating IFNγ, TNFα, and IL-17A in stage II HAT patients (similarly in both males and females) compared with healthy controls from the Democratic Republic of Congo (**Figure 4N**, **4O**, and **4P**, respectively), suggesting that this feature of infection is conserved between infected mice and humans.

IL-17A/F limits parasitaemia and clinical outcomes in male mice

Our results so far indicate that chronic iWAT infection leads to an expansion of Th17 effector T cells in male mice. However, the role of IL-17 on the control of *T. brucei* infection is not understood. To explore this, we used a global *Il17a/f* knockout mouse, which is deficient in both IL-17a and IL-17f (Haas et al., 2012). We monitored parasitaemia in male (**Figure 5A**) and female (**Figure 5B**) *Il17af*$^{-/-}$ mice over the course of infection. We observed that the first peak of parasitaemia was similar between wildtype and *Il17af*$^{-/-}$ male mice, but at late timepoints the *Il17af*$^{-/-}$ males displayed consistent higher levels of parasitaemia than their wildtype counterparts, indicating that IL-17A/F is essential to control infection during the chronic stage of the infection in male mice. In contrast, although not significant, the first peak of parasitaemia in *Il17af*$^{-/-}$ females was lower than in wild type mice, and the second peak of parasitaemia was delayed. Deletion of *Il17a/f* was also associated with an earlier onset and increased severity of clinical symptoms in both males (**Figure 5C**) and females (**Figure 5D**). *Il17af*$^{-/-}$ *m*ale and female mice started to exhibit clinical symptoms (piloerection and hunching) from 3 and 7 dpi, respectively, whereas wild type mice started to experience these symptoms between 12 and 15 dpi. Unlike bloodstream parasite numbers, the parasite burden of the major adipose tissue depots does not appear to be influenced by IL-17A/F in either sex (**Figure 5E and 5G**). Together, these findings suggest that IL-17A/F play a critical role in controlling

306 parasitaemia during the chronic stages of the infection, and in modulating clinical symptoms
307 in mice infected with *T. brucei*.

308 **IL-17A/F influences bodyweight and feeding behaviour in male mice during infection**

309 Our data so far indicate that chronic *T. brucei* infection leads to an accumulation of
310 T_H17 effector cells in the iWAT, as well as a significant increase of *Il17a* receptor expression,
311 indicating both local IL-17 production and a potential increase in IL-17A receptor signalling.
312 Therefore, we next asked whether IL-17A/F insufficiency leads to weight loss during infection.
313 As previously in this study, we monitored the weight of both male and female mice during the
314 course of infection. Unlike wild type male mice, infected *Il17af* knockout (*Il17af*$^{-/-}$) males
315 maintained their weight until 19 dpi, after which they started to gain significantly more weight
316 than infected wild type males (**Figure 6A**). In contrast, infected female *Il17af*$^{-/-}$ mice started to
317 gain weight in a similar pattern to wild type females, although similarly to males, knockout
318 females gained more weight that their wild type counterparts (**Figure 6B**). Some of this weight
319 gain was related to increased splenomegaly in *Il17af*$^{-/-}$ females, compared with their wild type
320 counterparts (**Supplementary Figure 2A**).

321 It was previously observed that when it is administered to wild type naïve mice, IL-17A
322 suppresses food intake (Nogueira et al., 2020). Therefore, to understand whether IL-17A
323 influences feeding behaviour and drives weight loss during infection, gross food intake was
324 measured for naïve and infected *Il17af*$^{-/-}$ mice. Until 9 dpi, wild type and *Il17af*$^{-/-}$ male mice
325 reduced their food intake at the same rate (**Figure 6C**). However, after 11dpi, *Il17af*$^{-/-}$ mice
326 started to increase their food intake above that of the wild types. Indeed, food intake for
327 infected *Il17af*$^{-/-}$ mice was higher between 15 and 23 dpi compared with at the onset of
328 infection. Unlike male mice, feeding behaviour was indistinguishable between infected female
329 *Il17af*$^{-/-}$ and wild type mice (**Figure 6D**). Together, this may suggest that IL-17A/F regulate
330 bodyweight by potentially suppressing the appetite of male mice during infection, but not
331 female mice. Further supporting this hypothesis, we found that naïve *I17af*$^{-/-}$ male mice have
332 significantly higher mass of iWAT than wild type males (**Figure 6E**), and this was not a result
333 of increased splenomegaly in this genotype compared with wild type males (**Supplementary**

Figure 2B). Upon infection, *Il17af*$^{-/-}$ knockout male mice also retained more of their iWAT mass compared with their wild type counterparts, suggesting that they experienced less wasting. In contrast to this, although naïve *I17af*$^{-/}$ female mice have a higher mass of iWAT than their wild type counterparts, they experience similar levels of wasting as wild type females upon infection (**Figure 6F**), supporting the assertion that the effects of IL-17A/F are sex-dependent.

To understand whether deletion of *Il17af*$^{-/-}$ impacts iWAT lipid content, we performed H&E staining on the iWAT (**Figure 6G**) and measured lipid droplet size in naïve and infected male (**Figure 6H**) and female (**Figure 6I**) mice and compared these with wild type animals. The iWAT adipocyte size was indistinguishable between genotypes in naïve animals. However, upon infection, *Il17af*$^{-/-}$ males retained a higher frequency of larger lipid droplets than wild type males (**Figure 6H**). When comparing this to female mice, we found that deletion of *Il17af*$^{-/-}$ had no impact on the range of lipid droplet sizes (**Figure 6I**). This observation indicates that IL-17A/F signalling drives lipid usage in adipocytes in males, but not in females, during infection. We reasoned that the changes in weight, feeding behaviour, and lipid usage may result from IL-17A signalling in the hypothalamus (Aviello et al., 2021), as adipose tissue function and feeding are centrally controlled by this brain structure (Zhang et al., 2014). Using single molecule fluorescence *in situ* hybridisation (smFISH), we observed transcription of *Il17ra*, the gene encoding the IL-17A receptor, in proximity to neurons in the arcuate nucleus of the hypothalamus in both naïve and infected male mice (**Figure 6J**). *Il17ra* expression occurred in proximity to neurons expressing agouti-related neuropeptide (*Agrp*) and pro-melanin concentrating hormone (*Pmch*), which are involved in promotion or suppression of feeding, respectively (Aponte et al., 2011). These observations suggest that the hypothalamus in general, and neurons controlling appetite and feeding behaviour in particular, are primed to sense IL-17 *via Il17ra*. In conjunction with increased levels of circulating IL-17A, we propose that during chronic infection with *T. brucei*, increased circulating levels of IL-17 lead to hypothalamic dysfunctions to suppress feeding, also driving weight loss in male mice.

Discussion

In this study, we wanted to understand the impact that African trypanosomes have on adipose tissue wasting in the subcutaneous adipose tissue depot, and whether this is mediated by components of the immune system. Throughout this study, we uncovered evidence demonstrating that male mice are more susceptible to trypanosomiasis-induced weight loss and adipose tissue wasting than female mice, and that IL-17A/F plays a key role in this sexually dimorphic pathology. Furthermore, we found that IL-17A/F suppresses food intake in males but not in females, potentially suggesting a dual effect of this cytokine; either locally in adipocytes, or in the hypothalamus to promote changes in feeding behaviour. Indeed, changes in feeding behaviour due to altered hypothalamic signalling may play a key role in the pathology that we observe during infection and may be an indirect consequence of perturbations within the central nervous system. Notably, we also observed elevation of circulating IL-17A in HAT patients, suggesting that this cytokine plays a role in the human immune response to *T. brucei* infection. It is, therefore, tempting to speculate that IL-17A could also play a role in mediating the weight loss experienced by patients infected with *T. brucei*.

Sexual dimorphism in the response to infection with *T. brucei*

Previous studies have focused primarily on the use of a single sex during *T. brucei* infection, with a limited number of studies comparing sexes when measuring effects on reproductive organs (Carvalho et al., 2018; Raheem, 2014). It is understood that males and females display multiple differential responses to infection, including differences in sickness behaviour (Vale and Jardine, 2015), weight loss (Cernetich et al., 2006), and the immune response (Klein and Flanagan, 2016). This aligns with the results presented here, where we observe differences in behaviour, weight loss and the immune response between male and female mice during infection. In the study presented here, weight loss in male mice was coupled with decreased iWAT mass. This was associated with a bigger decrease in adipocyte lipid droplet size in male than in female mice, potentially indicating that male mice utilise their lipid stores at a faster rate than females. Alternatively, this may be a result of females preferentially storing lipids in iWAT compared with males (Uranga et al., 2005), and so

throughout infection they are able to store more fatty acids obtained from their diet than males, slowing down lipid droplet shrinkage. Due to this loss of lipid content, we hypothesised that circulating glycerol, which is a proxy for measuring adipocyte lipolysis (Jansson et al., 1992), would be elevated during infection. However, we found that in both HAT patients and mice circulating glycerol levels are diminished during trypanosomiasis, supporting the idea that adipocytes become dysfunctional and limit their nutrient release. Decreased circulating glycerol may also occur as a result of adipocyte death, and so there are fewer adipocytes releasing nutrients into circulation. We speculate that since lipolysis is a critical regulator of multiple immune compartments, including macrophages (Kosteli et al., 2010) and $CD4^+$ T cells (Ioan-Facsinay et al., 2013), that downregulation of this pathway will also impair the immune response to infection. Further work is required to elucidate if this also takes places in African trypanosomiasis.

To further understand the processes driving the adipocyte shrinkage that we observed in male and female mice during infection, we performed bulk transcriptomic analyses on the iWAT. This supported our findings that adipose tissue lipolysis is diminished during infection, showing extensive downregulation of genes associated with mitochondrial metabolism and lipolysis in both males and females. This suppression of metabolic pathways has been observed in response to infection with other pathogens, such as *Mycobacterium tuberculosis* (Shi et al., 2015). During early *M. tuberculosis* infection of the lungs, transcripts encoding enzymes of oxidative phosphorylation and the tricarboxylic acid cycle are downregulated (Shi et al., 2015). Furthermore, in diseases such as anorexia nervosa, prolonged weight loss and negative energy balance, lipolysis decreases, which is hypothesised to preserve energy that is needed to maintain processes essential to survival (Xiao et al., 2020). In the context of sleeping sickness and nagana, prolonged weight loss may result in the adipose tissue shutting down its main metabolic functions to preserve energy, although we cannot rule out that this downregulation is caused by the loss of adipocytes and, and therefore, underrepresentation of transcripts from these cells.

Sexual dimorphism in the adipose tissue immune response to IL-17A/F during *T. brucei* infection

Previous studies of adipose tissue immune response focused exclusively on the gWAT of male mice, and identified an expansion of macrophage, Teff cell, and B cell populations (Carvalho et al., 2018). In agreement with this study, we also observed an expansion of macrophages and Teff cells. However, we also noted that there was a reduction in the proportion of B cells in the iWAT of male mice, and no changes in females, suggesting that this is a tissue- and sex-specific response.

Our observation that IL-17A signalling may be increased in mice and humans during infection with *T. brucei* led us to question whether this impacts adipose tissue structure and/or function. Genetic ablation of IL-17A and IL-17F prevented weight loss in *T. brucei*-infected male mice, but not in females, which gained weight over the course of infection to a similar rate to their wild type counterparts. This may be due to differences in feeding behaviour throughout the experiment, with *Il17af*$^{-/-}$ males eating more than wild type males, which is centrally regulated in the brain by the hypothalamus. Indeed, we observed an upregulation of *Il17ra* expression in both the iWAT and hypothalamus during chronic infection, and there is evidence to suggest that IL-17A influences food intake and feeding behaviour by acting on the hypothalamus under physiological conditions (Nogueira et al., 2020). The study by Nogueira *et al* (2020) supports our findings, as they also observed that IL-17A suppresses appetite, suggesting that IL-17A could play a central role in controlling sickness-induced anorexia during chronic infection.

IL-17 and adipose-hypothalamic interactions

As well as maintaining their weight, male *Il17af*$^{-/-}$ mice retained more of their adipose tissue and experienced less adipocyte hypotrophy than wild type males during infection. There are several plausible explanations for this. Studies of obesity have found that IL-17-producing mucosal-associated invariant T (MAIT) cells are enriched in the adipose tissue of obese children (Carolan et al., 2015), and may influence insulin signalling (Bergin et al., 2022). Zúñiga et al (2010) found that IL-17 deficient male mice were more insulin sensitive than wild

types, which may limit lipolysis due to the anti-lipolytic effects of insulin signalling (Jensen, 1995). However, it remains unclear which IL-17 isoform led to this effect. Conversely, human studies suggest that decreased concentrations of circulating IL-17A and IL-17F lead to insulin resistance (Zhou et al., 2020). This disparity may result from knockout of other isoforms of IL-17 in mice, or it may indicate that the role of IL-17 in modulating metabolism is context dependent. Alternatively, it is now appreciated that IL-17-producing gamma-delta (γδ) T cells play a physiological role in control of body temperature and adipose tissue immune homeostasis (Hu et al., 2020). During cold exposure, the frequency of IL-17A-producing γδ T cells in the brown adipose tissue increases and promotes non-shivering thermogenesis, whereby the tissue consumes fuel to generate heat (Kohlgruber et al., 2018). It is tempting to speculate that during early *T. brucei* infection, mice switch on their thermogenic program, which contributes to fever generation (Yoneshiro et al., 2021), and this may contribute to additional consumption of lipids in the adipose tissue. Recent studies identified that agouti-related neuropeptide (AGRP; encoded by *Agrp*)-producing neurons in the hypothalamus, which promote feeding contribute to the activation of adipose tissue thermogenesis, and that this, in turn, can influence bodyweight (Han et al., 2021). Further to this, pro-opiomelanocortin (POMC; encoded by *Pmch*)-positive neurons, which suppress feeding, can also promote thermogenesis (Yao et al., 2017). Differential activation of these neurons, therefore, influence the weight of an organism, and their adipose tissue mass. In the context of infection, IL-17A signalling in the hypothalamus drives POMC expression and, with prolonged exposure, AGRP expression (Nogueira et al., 2020). This temporal response to IL-17A suggests that during *T. brucei* infection, at early timepoints there is an increase in the activity of POMC-expressing neurons, leading to suppressed food intake, whilst at later timepoints there may be an increase in the activity of AGRP-expressing neurons. However, further studies are required to determine this.

Based on all these observations, we propose a model whereby chronic *T. brucei* infection leads to an increase in circulating IL-17A/F in humans and animals, which might act locally in the adipose tissue, by direct signalling through the IL-17 receptor to promote

adipocyte lipolysis, as well as in the hypothalamus to modulate feeding behaviour in a sex-dependent manner. Further work genetically manipulating IL-17 signalling in a cell- and/or tissue-specific manner might provide further mechanistic insights into this process. This study provides insights into the metabolic response of adipose tissue during infection with *T. brucei* and how changes in cellular metabolism influence systemic metabolism. Furthermore, this work highlights the sex-dependent effects of IL-17A/F on the adipose tissue responses to infection. Future work is needed to determine the pathways underpinning these sex differences, as well as the potential sources of IL-17A/F during infection, which has implications for sexually dimorphic responses to infectious diseases in humans.

Figure Legends

Figure 1. Male mice lose weight during infection with *Trypanosoma brucei*, which is associated with alterations in feeding behaviour. (A) Number of parasites per mL of blood, measured using phase microscopy and the rapid "matching" method (Herbert and Lumsden, 1976). **(B)** Clinical scores of infected male and female mice. **(C)** Percentage changes in body weight of male and **(D)** female mice over the course of infection. Percentage changes in food intake in male **(E)** and female **(F)** mice. Each data point represents 2 cages (*n*=3-4 mice per cage). Time series data were analysed using two-way repeated measures ANOVA with Sidak post-hoc testing and are expressed as mean ±SD. **p*<0.05, ***p*<0.01, ****p*<0.001, ns = non-significant.

Figure 2. *Trypanosoma brucei* infection leads to reductions in iWAT mass and lipid content, as well as impairment of adipose tissue function. (A) Schematic highlighting the anatomical location of the inguinal white adipose tissue (iWAT). **(B)** Histological analysis of the iWAT and gWAT trypanosome colonisation, using HSP70 staining**. (C)** Parasite burden of iWAT and gWAT**.** Parasite density in the iWAT, which was measured by RT-qPCR of genomic DNA. A comparison was made with gonadal white adipose tissue (gWAT), to understand if the iWAT is also highly colonised. **(D)** iWAT mass at 25 days post-infection or in naïve mice. iWAT was dissected and weighed before normalising to body weight, to account for variation between biological replicates. Symbols indicate the number of biological replicates collected from two independent experiments **(E)** Representative histological H&E staining of iWAT showing adipocyte lipid droplets and immune infiltrate. Magnification = 20X. Insets highlight likely immune cell infiltrate. **(F)** Analysis of lipid droplet area (μm^2) in naïve and infected males and **(G)** females. *N*=6 biological replicates per group, from two independent experiments. Lipid droplets were measured from 3 distinct areas in each image and then combined for each biological replicate. **(H)** Circulating glycerol concentration in naïve vs. infected male and female mice. *n*=4 biological replicates per group. **(I)** Circulating glycerol concentration in healthy vs. infected patients. *N*=5 patients per group and each group is a mix of male and

female. For **C**, **D, H** and **I**, data were analysed using a two-tailed Student t test. For **F** and **G**, data were analysed using a two-way ANOVA with Sidak post-hoc testing. Data for all panels are expressed as mean ±SD. *p<0.05, **p<0.01, ***p<0.001, ****p<0.0001, ns = non-significant.

Figure 3. Transcriptomic analysis suggests a stronger T cell response in the iWAT of males than females. (A) Principal component analysis of bulk transcriptomic data from male and female naïve and infected mice. **(B)** Venn diagram of genes that were upregulated in infected male and female mice compared with naïve controls, highlighting the number of overlapping or non-overlapping genes. **(C)** Heatmap of the 25 most significantly dysregulated genes during infection. Both naïve and infected groups contain an even number of males and females. **(D)** Heatmap of T_H17 transcripts in male mice. n=4 biological replicates per group.

Figure 4. Elevated circulating IL-17A is associated with increased IL-17 receptor A (IL-17RA) in male mice during *T. brucei* infection. (A) Measurements of the proportions of B cells, **(B)** macrophages, **(C)** granulocytes, and **(D)** dendritic cells. **(E)** Representative viSNE plots highlighting the gating strategy for analysis of $CD4^+$ cells. We gated on CD45+, CD3ε, TCRβ, CD4+ cells. **(F)** Measurements of the proportions of $CD4^+$, **(G)** T effector (Teff), **(H)** IFNγ-producing and **(I)** IL-17A-producing T cells. **(J)** Expression of interleukin-17A receptor (*Il17ra*) mRNA in infected male and female mice. Measurements of circulating serum IL-17A, TNFa, and IFNγ in mice **(K**, **L**, **M)** and IFNγ, TNFa and total IL-17 in humans **(N**, **O**, **P)**. Mouse cytokine data were collected from samples taken across three independent experiments. Data were tested for normal distribution and analysed by either one-way ANOVA or a Kruskal Wallis test. Biological replicates are indicated by symbols for each panel. Data points indicate biological replicates for each panel. Data for all panels are expressed as mean ±SD. *p<0.05, **p<0.01, ***p<0.001, ****p<0.0001, ns = non-significant.

Figure 5. IL-17A/F limits parasitaemia and clinical symptoms during *T. brucei* infection. Number of parasites per mL of blood in *Il17af*$^{-/-}$ vs wild type male **(A)** and female **(B)** mice, which was measured using phase microscopy and the rapid "matching" method (Herbert and Lumsden, 1976). **(C** and **D)** Parasite burden of iWAT and gWAT. **(E** and **F)** Clinical scores of infected male and female mice. iWAT = inguinal white adipose tissue; gWAT = gonadal white adipose tissue; BAT = brown adipose tissue. Symbols indicate the number of biological replicates per group. Data are expressed as mean ±SD. **p*<0.05, ***p*<0.01, ns = non-significant.

Figure 6. Deletion of *Il17a* and *Il17f* limits weight loss and adipose tissue wasting, and alters feeding behaviour in males infected with *Trypanosoma brucei*. (A) Percentage changes in bodyweight of wild type and *Il17af*$^{-/-}$ male mice over the course of infection. *n*=7 mice per group across two independent experiments. **(B)** Percentage weight changes in bodyweight of wild type and *Il17af-/-* female mice over the course of infection. **(C and D**) Changes in gross food intake over the course of infection. Each data point represents 2 cages (*n*=3-4 mice per condition) from 2 independent experiments. **(E)** iWAT mass in naïve wild type and *Il17af-/-* male mice. **(F)** iWAT mass in naïve wild type and *Il17af-/-* female mice. **(G)** H&E staining of iWAT from male and female *Il17af*$^{-/-}$ mice. Analysis of lipid droplet area (μm^2) in naïve and infected males **(H)** and **(I)**. Lipid droplets were measured from 3 distinct areas in each image and then combined for each biological replicate. **(J)** Single molecule fluorescence *in situ* hybridisation imaging of the hypothalamus from naïve and infected male C57BL/6 mice. IIIV = 3rd ventricle; β1 and β2 = tanycytes; ARH = arcuate nucleus of the hypothalamus; *Agrp* = agouti-related neuropeptide; *Pmch* = pro-melanin concentrating hormone; *Il17ra* = IL-17A receptor. Data for wild type mice in panels **A, B, C**, and **D** are taken from Figure 1. Data for wild type mice in panels **E, F, G,** and **H** are taken from Figure 3. Data in panels **A, B, C,** and **D** were analysed using two-way repeated measures ANOVA with Sidak post-hoc testing. Data in panels **E** and **F** were analysed using one-way ANOVA with Tukey post-hoc testing. Data points represent biological replicates. Data in panels **A** – **I** are from 2-3 independent

583 experiments. Data are expressed as ±SD. **p<0.01, ***p<0.001, ****p<0.0001, ns = non-
584 significant
585
586 **Supplementary Figure Legends**
587 **Supplementary Figure 1, related to Figure 2. Spleen mass increases in both male and**
588 **female mice during infection.** Spleen weights were normalised to bodyweight and the fold
589 change in weight calculated. Each point represents a biological replicate. Data were analysed
590 using one-way ANOVA with Tukey post-hoc testing. ****p<0.0001.
591
592 **Supplementary Figure 2, related to Figure 6. Spleen mass is higher in *Il17af*$^{-/-}$ than wt**
593 **females during infection.** Spleen weights from males **(A)** and females **(B)** were normalised
594 to bodyweight and the fold change in weight calculated. Each point represents a biological
595 replicate. Data were analysed using one-way ANOVA with Tukey post-hoc testing.
596 ****p<0.0001.
597
598
599
600
601
602
603
604
605
606
607
608
609
610

Materials & Methods

Ethics statement

Human serum samples used for glycerol measurements were collected in Guinea as part of the National Control Program. Participants were informed of the study objectives in their own language and signed a written consent form. Human serum samples used for IL-17A measurements were collected as part of the TrypanoGEN Biobank, with ethical approval from the Democratic Republic of Congo National Ministry of Public Health (approval number 1/2013). Samples were used from different regions due to limitations in sample availability. Ethical approval to use all human samples outlined in this study was given by the University of Glasgow (Project No: 200120043). All animal experiments were approved by the University of Glasgow Ethical Review Committee and performed in accordance with the home office guidelines, UK Animals (Scientific Procedures) Act, 1986 and EU directive 2010/63/EU. All experiments were conducted under SAPO regulations and UK Home Office project licence number PC8C3B25C to Dr Jean Rodgers.

Murine infections with *Trypanosoma brucei*

Six to eight weeks old male or female C57Black/6Jm (JAX, stock 000664) or *Il17af*$^{-/-}$ (stock 034140, The Jackson Laboratory, Maine, USA) mice were inoculated by intra-peritoneal injection with ~2 x 10^3 parasites of strain *T. brucei brucei* Antat 1.1^E (Le Ray et al., 1977). Parasitaemia was monitored by regular sampling from tail venesection and examined using phase microscopy and the rapid “matching” method (Herbert and Lumsden, 1976). Uninfected mice of the same strain, sex and age served as uninfected controls. All mice were fed *ad libitum* and kept on a 12 h light–dark cycle. All *in vivo* experiments were concluded at 25 days post-infection, to model chronic infection in humans.

RNA Purification

iWAT was harvested from mice and stored in TRIzol™ (Cat. #15596026, Invitrogen, Massachusetts, USA). Total RNA was then purified from iWAT using an RNeasy Kit (Cat. #74004, Qiagen, Dusseldorf, Germany) as per the manufacturer’s recommendations. The RNA was purified in 30 µL of nuclease-free water (Cat. #129112, Qiagen, Dusseldorf,

Germany), and RNA concentration measured on a NanoDrop™ 2000 (Cat. #ND2000, Thermo Fisher Scientific, Massachusetts, USA). Samples were shipped to Novogene (Cambridge, UK) to undergo quality control, library preparation and sequencing. RNA integrity was assessed using an RNA Nano 6000 Assay Kit (Cat. # 5067-1511, Agilent Technologies, California, USA) with a Bioanalyzer 2100 (Agilent Technologies, California, USA), as per the manufacturer's instructions. Samples with an RNA integrity number (RIN) of >6.0 were qualified for RNA sequencing.

Library Preparation

Library preparation was performed by Novogene (Cambridge, UK). Messenger RNA (mRNA) was purified from total RNA using poly-T oligo-attached magnetic beads. Fragmentation was carried out using divalent cations under elevated temperature in a First Strand Synthesis Reaction Buffer (5X). First strand cDNA was synthesized using random hexamer primers and M-MuLV Reverse Transcriptase (RNase H-). Second strand cDNA synthesis was then performed using DNA Polymerase I and RNase H. Remaining overhangs were converted to blunt ends *via* exonuclease/polymerase activity. Following adenylation of 3' ends of DNA fragments, adaptors with hairpin loop structures were ligated. To select cDNA fragments of 370~420 bp in length, library fragments were purified using AMPure XP beads (Beckman Coulter, Beverly, USA), as per the manufacturer's instructions. PCR was then performed using Phusion High-Fidelity DNA polymerase, Universal PCR primers, and Index (X) primers. Finally, PCR products were purified (AMPure XP system) using AMPure XP beads (Beckman Coulter, Beverly, USA), as per the manufacturer's instructions, and library quality was assessed using a Bioanalyzer 2100 (Agilent Technologies, CA, USA).

Sequencing and data analysis

Clustering of the index-coded samples was performed on a cBot Cluster Generation System using a TruSeq PE Cluster Kit v3-cBot-HS (Illumia, California, USA) according to the manufacturer's instructions. After cluster generation, libraries were sequenced on an Illumina Novaseq platform and 150 bp paired-end reads were generated. Raw reads in fastq format were processed through proprietary Perl scripts developed by Novogene (Cambridge, UK).

Clean reads were obtained by removing reads containing adapters, poly-N, or low-quality reads from raw data. Concurrently, the Q20, Q30 and GC content of the clean data was calculated. Genome and genome annotation files (Genome Reference Consortium Mouse Build; GRCm39) were downloaded. An index of the reference genome was built using Hisat2 v2.0.5 and paired-end clean reads were aligned to the reference genome using Hisat2 v2.0.5. The featureCounts (v. 1.5.0-p3) package was used to count read numbers mapped to each gene, before calculating the Fragments Per Kilobase of transcript sequence per Millions base pairs (FPKM) of each gene using the length of the gene and reads count mapped to this gene. Differential expression analysis was performed using the DESeq2 R package (v. 1.20.0). DESeq2 The resulting *p*-values were adjusted using the Benjamini and Hochberg approach to control false discovery rate. Genes with an adjusted *p*-value of <0.05 were assigned as differentially expressed. Pathway enrichment analysis of differentially expressed genes was performed using the ShinyGO (v. 0.76) package (Ge et al., 2020), mapping genes to the Kyoto Encyclopaedia of of Genes and Genomes (KEGG) database (Kanehisa et al., 2021). KEGG terms with an adjusted *p*-value <0.05 were considered significantly enriched. Heatmaps were generated using the pheatmap (Version 1.0.12) and Tidyverse (Wickham et al., 2019) packages in R (Version 4.2.1). Samples were clustered by Euclidean distance.

DNA Purification

Tissues were harvested from mice and snap frozen. Tissue was digested using a DNeasy Blood and Tissue kit (Cat. #69504, Qiagen, Dusseldorf, Germany), before purifying DNA as per the manufacturer's instructions. DNA was eluted in 100 µL of EB buffer (Cat. # 19086, Qiagen, Dusseldorf, Germany).

Tissue Parasite Burden Quantification

To quantify *T. brucei* parasites in tissue, we amplified 18S ribosomal DNA genes from the gDNA of a known mass of tissue, using qRT-PCR Brilliant II Probe Master Mix (Cat. #600809, Agilent Technologies, California, USA) with a TaqMan™ TAMRA Probe system (Cat. #450025, Applied Biosystems, Massachusetts, USA). Primer sequences were specific to *T. brucei* 18S ribosomal DNA (**Table 1**). The cycling conditions used for qRT-PCR are

outlined in **Table 2**. Generated data was converted to parasite copy number using a standard curve.

Primer/probe name	Primer/probe sequence
TBPFR Forward Taqman primer	CCA ACC GTG TGT TTC CTC CT
TBPFR Reverse Taqman primer	CGG CAG TAG TTT GAC ACC TTT TC
TBPFR probe	5'-FAM CTT GTC TTC TCC TTT TTT GTC TCT TTC CCC CT 3'TAMRA

Table 1. Primer and probe sequences for tissue parasite burden quantification

Step	Temperature	Time	Number of cycles
1	95	10 minutes	1
2	95	15 seconds	45
3	60	1 minutes	
4	72	1 seconds	

Table 2. Thermal cycling conditions for tissue parasite burden quantification

Histological Analyses

Tissues were placed into 4% paraformaldehyde (PFA) and fixed overnight at room temperature. PFA-fixed tissues were then embedded in paraffin, sectioned, and stained by the Veterinary Diagnostic Services facility (University of Glasgow, UK). Sections were Haematoxylin and Eosin (H&E) stained for lipid droplet measurement analysis, or 3'-diaminobenzidine (DAB) stained for heat-shock protein 70 (HSP70) to detect *T. brucei* parasites. The HSP70 antibody was a kind gift from Professor James D. Bangs. Slide imaging was performed by the Veterinary Diagnostic Services facility (University of Glasgow, UK) using an EasyScan Infinity slide scanner (Motic, Hong Kong) at 20X magnification. To determine lipid droplet sizes in adipose tissue, images were first opened in QuPath (v. 0.3.2) (Bankhead et al., 2017), before selecting regions and exporting to Fiji (Schindelin et al., 2012). In Fiji,

images were converted to 16-bit format, and we used the Adiposoft plugin to quantify lipid droplet area within different sections.

Immunofluorescence and single molecule fluorescence *in situ* hybridisation (smFISH) using RNAscope

To prepare tissue sections for smFISH, infected animals and naïve controls were anesthetized with isoflurane, brains were dissected out into 4% PFA. Following overnight fixation in 4% PFA, tissues were embedded in paraffin, and sectioned by the Veterinary Diagnostic Services facility (University of Glasgow, Glasgow, UK). An RNAscope 2.5 Assay (Advanced Cell Diagnostics, California, USA) was used for all smFISH experiments, according to the manufacturer's protocols. All RNAscope smFISH probes (**Table 3**) were designed and validated by Advanced Cell Diagnostics. For image acquisition, 16-bit laser scanned confocal images were acquired using the 63x/1.4 plan-apochromat objective of an LSM 880 confocal microscope (Zeiss, Oberkochen, Germany). smFISH images were acquired with minor contrast adjustments as needed, and converted to grayscale, to maintain image consistency. The resulting images were processed and analysed using Fiji (Schindelin et al., 2012), and the values plotted using GraphPad Prism (v. 8.0).

List of RNAScope probes used for smFISH			
***Mus musculus* probes**			
Supplier	**Catalogue number**	**Sequence**	**Channel**
Biotechne	403741	Mm-*Il17ra*	Channel 1
Biotechne	478728-C2	Mm-*Pmch*	Channel 2
Biotechne	400711-C4	Mm-*Agrp*	Channel 4

Table 3 smFISH probes used for RNAScope

Mass cytometry sample processing

Adipose tissue was dissected out and transferred to PBS, before dissociating using an Adipose Tissue Dissociation Kit for Mouse and Rat (Cat. # 130-105-808, Miltenyi Biotec, Cologne, Germany), using a gentleMACS™ Octo Dissociator with Heaters (Cat. #130-096-

427, Miltenyi Biotec, Cologne, Germany), as per the manufacturer's recommendations. After the final recommended centrifugation, the pellet (containing the immune cells) was resuspended in Dubecco's Modified Eagle Medium (DMEM) to a concentration of 1 x 10^6 cells/mL. Cells were activated for 6 h in a round-bottom 96-well plate using Cell Activation Cocktail (with Brefeldin A) (Cat. #423304, BioLegend, San Diego, USA) as per the manufacturer's recommendations. Plates were then centrifuged at 300 x g for 5 min and the pellets resuspended in 50 µL of Cell-ID™ Cisplatin-195Pt viability reagent (Cat. # 201195, Standard BioTools, San Francisco, USA), and incubated at room temperature for 2 min. Cells were washed twice in Maxpar® Cell Staining Buffer (Cat. # 201068, Standard BioTools, San Francisco, USA), and centrifuged at 300 x g at room temperature for 5 min. The CD16/CD32 receptors were then blocked by incubating with a 1/50 dilution of TruStain FcX™ (Cat. #101319, BioLegend, San Diego, USA) in PBS at room temperature for 15 min. An antibody cocktail was prepared (**Table 4**) from the Maxpar® Mouse Sp/LN Phenotyping Panel Kit (Cat. #201306, Standard BioTools, San Francisco, USA), with additional antibodies against IL-17A, IFNγ, TCRgd, and CD27 included (**Table 4**). Cells were incubated with antibodies (**Table 4**) for 60 min, on ice before washing 3 times in Maxpar® Cell Staining Buffer (Cat. # 201068, Standard BioTools, San Francisco, USA) as previously.

Following staining, cells were fixed in 2% paraformaldehyde (PFA) overnight at 4°C. Cells were then washed twice with 1 x eBioscience™ Permeabilization Buffer (Cat. #00-8333-56, Invitrogen, Waltham, USA) at 800 x g at room temperature for 5 min. The pellets were resuspended in intracellular antibody cocktail (**Table 4**) and incubated at room temperature for 45 min. Cells were washed 3 times in Maxpar® Cell Staining Buffer (Cat. # 201068, Standard BioTools, San Francisco, USA) at 800 x g. The cells were then resuspended in 4% PFA at room temperature for 15 min, before collecting the cells at 800 x g and resuspending in Cell-ID™ Intercalator-Ir (Cat. # 201192A, Standard BioTools, San Francisco, USA). Finally, the cells were barcoded by transferring the stained cells to a fresh tube containing 2 µL of palladium barcode from the Cell-ID™ 20-Plex Pd Barcoding Kit (Cat. # 201060, Standard

BioTools, San Francisco, USA). Cells were then frozen in a freezing solution (90% FBS and 10% DMSO), before shipping to the Flow Cytometry Core Facility at the University of Manchester for data acquisition.

Surface Antibodies				
Antibody	**Metal Conjugate**	**Clone**	**Concentration**	**Cat. No.**
Ly6G/C [Gr1]	141Pr	RB6-8C5	1/100	201306
CD11c	142Nd	N418	1/100	
CD69	145Nd	H1.2F3	1/100	
CD45	147Sm	30-F11	1/200	
CD11b	148Nd	M1/70	1/100	
CD19	149Sm	6D5	1/100	
CD3e	152Sm	145-2C11	1/100	
TCRβ	169Tm	H57-597	1/100	
CD44	171Yb	IM7	1/100	
CD4	172Yb	RM4-5	1/100	
Intracellular Antibodies				
IL-17A	174Yb	TC11-18H10.1	1/100	3174002C
IFNγ	165Ho	XMG1.2	1/100	3165003B

Table 4 Antibodies for mass cytometry

Quantification of cytokine titres

To measure cytokine titres in murine serum samples we used a U-PLEX Biomarker kit (Meso Scale Discovery, Rockville, USA), as per the manufacturer's instructions. Samples were analysed using a MESO QuickPlex SQ 120 (Meso Scale Discovery, Rockville, USA). IL-17A titres in human serum samples were quantified using a multiplex cytokine panel (M500KCAF0Y; Bio-Plex Pro Human Cytokine Assay (BioRad) and a LuminexCorp Luminex 100 machine as per the manufacturer's instructions.

769 **Statistical analyses**

770 All statistical analyses were performed using Graph Prism Version 8.0 for Windows or
771 macOS, GraphPad Software (La Jolla California USA). Normality of data distribution was
772 measured using the Shapiro-Wilks test. Where indicated, data were analysed by unpaired
773 Student's t-test, Mann-Whitney test, one-way analysis of variance (ANOVA) or two-way
774 ANOVA. Data were considered to be significant where $p < 0.05$.

775 **Data Availability**

776 The GEO accession number for transcriptomic sequencing data reported in this paper
777 is: GSE21060.

778 **Acknowledgements**

779 We firstly thank the TrypanoGEN Network for providing serum samples from patients.
780 We also thank Jean Rodgers for the use of her project licence for performing animal work. We
781 thank the Histology Research Service at Veterinary Diagnostic Services, School of Veterinary
782 Medicine, University of Glasgow. We also thank Nicola Munro, Scott McCall and Catrina Boyd
783 at the Veterinary Research Facility (University of Glasgow) for maintaining optimal husbandry
784 conditions and comfort for the animals used in this study. Finally, the authors would like to
785 thank the Flow Cytometry Core Facility, University of Manchester, UK, for mass cytometry
786 sample acquisition. This work was funded in part by a Wellcome Trust Institutional Strategic
787 Support Fund and Society for Endocrinology Early Career Grant to MCS. This work was also
788 funded in part by a Wellcome Trust Senior Research Fellowship [209511/Z/17/Z] awarded to
789 AML. JFQ is funded by a Sir Henry Wellcome postdoctoral fellowship (221640/Z/20/Z to JFQ).
790 PC is funded by Wellcome Centre for Integrative Parasitology FutureScope grant to JFQ
791 [310358-01]. GPW is funded by an MRC grant (MR/S009779/1). CB is funded by an MRC
792 grant [MR/W018497/1]. SK is funded by the National Institute of Diabetes and Digestive and
793 Kidney Diseases and the Howard Hughes Medical Institute. The authors declare that the
794 research was conducted in the absence of any commercial or financial relationships that could
795 be construed as a potential conflict of interest.

796

Bibliography

Adelman JS, Martin LB. 2009. Vertebrate sickness behaviors: Adaptive and integrated neuroendocrine immune responses. *Integr Comp Biol* **49**:202–214. doi:10.1093/ICB/ICP028

Aponte Y, Atasoy D, Sternson SM. 2011. AGRP neurons are sufficient to orchestrate feeding behavior rapidly and without training. *Nat Neurosci* **14**:351. doi:10.1038/NN.2739

Aviello G, Cristiano C, Luckman SM, D'Agostino G. 2021. Brain control of appetite during sickness. *Br J Pharmacol* **178**:2096–2110. doi:10.1111/BPH.15189

Baazim H, Antonio-Herrera L, Bergthaler A. 2022. The interplay of immunology and cachexia in infection and cancer. *Nat Rev Immunol* **22**:309–321. doi:10.1038/S41577-021-00624-W

Bankhead P, Loughrey MB, Fernández JA, Dombrowski Y, McArt DG, Dunne PD, McQuaid S, Gray RT, Murray LJ, Coleman HG, James JA, Salto-Tellez M, Hamilton PW. 2017. QuPath: Open source software for digital pathology image analysis. *Scientific Reports 2017 7:1* **7**:1–7. doi:10.1038/s41598-017-17204-5

Bergin R, Kinlen D, Kedia-Mehta N, Hayes E, Cassidy FC, Cody D, O'Shea D, Hogan AE. 2022. Mucosal-associated invariant T cells are associated with insulin resistance in childhood obesity, and disrupt insulin signalling via IL-17. *Diabetologia* **65**:1012–1017. doi:10.1007/S00125-022-05682-W/FIGURES/2

Bukachi SA, Wandibba S, Nyamongo IK. 2017. The socio-economic burden of human African trypanosomiasis and the coping strategies of households in the South Western Kenya foci. *PLoS Negl Trop Dis* **11**. doi:10.1371/JOURNAL.PNTD.0006002

Cabalén ME, Cabral MF, Sanmarco LM, Andrada MC, Onofrio LI, Ponce NE, Aoki MP, Gea S, Cano RC. 2016. Chronic Trypanosoma cruzi infection potentiates adipose tissue macrophage polarization toward an anti-inflammatory M2 phenotype and contributes to diabetes progression in a diet-induced obesity model. *Oncotarget* **7**:13400. doi:10.18632/ONCOTARGET.7630

Capewell P, Cren-Travaillé C, Marchesi F, Johnston P, Clucas C, Benson RA, Gorman TA, Calvo-Alvarez E, Crouzols A, Jouvion G, Jamonneau V, Weir W, Lynn Stevenson M, O'Neill K, Cooper A, Swar NRK, Bucheton B, Ngoyi DM, Garside P, Rotureau B, MacLeod A. 2016. The skin is a significant but overlooked anatomical reservoir for vector-borne African trypanosomes. *Elife* **5**. doi:10.7554/eLife.17716

Carolan E, Tobin LM, Mangan BA, Corrigan M, Gaoatswe G, Byrne G, Geoghegan J, Cody D, O'Connell J, Winter DC, Doherty DG, Lynch L, O'Shea D, Hogan AE. 2015. Altered distribution and increased IL-17 production by mucosal-associated invariant T cells in adult and childhood obesity. *J Immunol* **194**:5775–5780. doi:10.4049/JIMMUNOL.1402945

Carvalho T, Trindade S, Pimenta S, Santos AB, Rijo-Ferreira F, Figueiredo LM. 2018. Trypanosoma brucei triggers a marked immune response in male reproductive organs. *PLoS Negl Trop Dis* **12**. doi:10.1371/JOURNAL.PNTD.0006690

Cernetich A, Garver LS, Jedlicka AE, Klein PW, Kumar N, Scott AL, Klein SL. 2006. Involvement of gonadal steroids and gamma interferon in sex differences in response to blood-stage malaria infection. *Infect Immun* **74**:3190–3203. doi:10.1128/IAI.00008-06/SUPPL_FILE/TABLE_S3.DOC

Childs CE, Calder PC, Miles EA. 2019. Diet and Immune Function. *Nutrients* **11**. doi:10.3390/NU11081933

Choe SS, Huh JY, Hwang IJ, Kim JI, Kim JB. 2016. Adipose tissue remodeling: Its role in energy metabolism and metabolic disorders. *Front Endocrinol (Lausanne)* **7**:30. doi:10.3389/FENDO.2016.00030/BIBTEX

Chusyd DE, Wang D, Huffman DM, Nagy TR. 2016. Relationships between Rodent White Adipose Fat Pads and Human White Adipose Fat Depots. *Front Nutr* **3**:1. doi:10.3389/FNUT.2016.00010

Dahlman I, Mejhert N, Linder K, Agustsson T, Mutch DM, Kulyte A, Isaksson B, Permert J, Petrovic N, Nedergaard J, Sjölin E, Brodin D, Clement K, Dahlman-Wright K, Rydén M,

Arner P. 2010. Adipose tissue pathways involved in weight loss of cancer cachexia. *Br J Cancer* **102**:1541. doi:10.1038/SJ.BJC.6605665

Duncan RE, Ahmadian M, Jaworski K, Sarkadi-Nagy E, Sul HS. 2007. Regulation of Lipolysis in Adipocytes. *Annu Rev Nutr* **27**:79. doi:10.1146/ANNUREV.NUTR.27.061406.093734

Finn PF, Dice JF. 2006. Proteolytic and lipolytic responses to starvation. *Nutrition* **22**:830–844. doi:10.1016/J.NUT.2006.04.008

Galarraga M, Campión J, Munõz-Barrutia A, Boqué N, Moreno H, Martínez JA, Milagro F, Ortiz-de-Solórzano C. 2012. Adiposoft: automated software for the analysis of white adipose tissue cellularity in histological sections. *J Lipid Res* **53**:2791–2796. doi:10.1194/JLR.D023788

Ge SX, Jung D, Jung D, Yao R. 2020. ShinyGO: a graphical gene-set enrichment tool for animals and plants. *Bioinformatics* **36**:2628–2629. doi:10.1093/BIOINFORMATICS/BTZ931

Guedes PMDM, Gutierrez FRS, Maia FL, Milanezi CM, Silva GK, Pavanelli WR, Silva JS. 2010. IL-17 Produced during Trypanosoma cruzi Infection Plays a Central Role in Regulating Parasite-Induced Myocarditis. *PLoS Negl Trop Dis* **4**. doi:10.1371/JOURNAL.PNTD.0000604

Haas JD, Ravens S, Düber S, Sandrock I, Oberdörfer L, Kashani E, Chennupati V, Föhse L, Naumann R, Weiss S, Krueger A, Förster R, Prinz I. 2012. Development of Interleukin-17-Producing γδ T Cells Is Restricted to a Functional Embryonic Wave. *Immunity* **37**:48–59. doi:10.1016/j.immuni.2012.06.003

Han Y, Xia G, Srisai D, Meng F, He Yanlin, Ran Y, He Yang, Farias M, Hoang G, Tóth I, Dietrich MO, Chen MH, Xu Y, Wu Q. 2021. Deciphering an AgRP-serotoninergic neural circuit in distinct control of energy metabolism from feeding. *Nature Communications 2021 12:1* **12**:1–16. doi:10.1038/s41467-021-23846-x

Herbert WJ, Lumsden WHR. 1976. Trypanosoma brucei: A rapid "matching" method for estimating the host's parasitemia. *Exp Parasitol* **40**:427–431. doi:10.1016/0014-4894(76)90110-7

Hu B, Jin C, Zeng X, Resch JM, Jedrychowski MP, Yang Z, Desai BN, Banks AS, Lowell BB, Mathis D, Spiegelman BM. 2020. γδ T cells and adipocyte IL-17RC control fat innervation and thermogenesis. *Nature 2020 578:7796* **578**:610–614. doi:10.1038/s41586-020-2028-z

Hube F, Hauner H. 1999. The role of TNF-alpha in human adipose tissue: prevention of weight gain at the expense of insulin resistance? *Horm Metab Res* **31**:626–631. doi:10.1055/S-2007-978810

Ioan-Facsinay A, Kwekkeboom JC, Westhoff S, Giera M, Rombouts Y, van Harmelen V, Huizinga TWJ, Deelder A, Kloppenburg M, Toes REM. 2013. Adipocyte-derived lipids modulate CD4+ T-cell function. *Eur J Immunol* **43**:1578–1587. doi:10.1002/EJI.201243096

Jansson PA, Larsson A, Smith U, Lönnroth P. 1992. Glycerol production in subcutaneous adipose tissue in lean and obese humans. *J Clin Invest* **89**:1610–1617. doi:10.1172/JCI115756

Jensen MD. 1995. Gender differences in regional fatty acid metabolism before and after meal ingestion. *J Clin Invest* **96**:2297–2303. doi:10.1172/JCI118285

Kanehisa M, Furumichi M, Sato Y, Ishiguro-Watanabe M, Tanabe M. 2021. KEGG: integrating viruses and cellular organisms. *Nucleic Acids Res* **49**:D545–D551. doi:10.1093/NAR/GKAA970

Kennedy PGE. 2019. Update on human African trypanosomiasis (sleeping sickness). *J Neurol* **266**:2334–2337. doi:10.1007/S00415-019-09425-7

Kennedy PGE. 2013. Clinical features, diagnosis, and treatment of human African trypanosomiasis (sleeping sickness). *Lancet Neurol* **12**:186–194. doi:10.1016/S1474-4422(12)70296-X

Klein SL, Flanagan KL. 2016. Sex differences in immune responses. *Nature Reviews Immunology 2016 16:10* **16**:626–638. doi:10.1038/nri.2016.90

Kohlgruber AC, Gal-Oz ST, Lamarche NM, Shimazaki M, Duquette D, Nguyen HN, Mina AI, Paras T, Tavakkoli A, von Andrian U, Banks AS, Shay T, Brenner MB, Lynch L. 2018. γδ T cells producing interleukin-17A regulate adipose regulatory T cell homeostasis and thermogenesis. *Nature Immunology 2018 19:5* **19**:464–474. doi:10.1038/s41590-018-0094-2

Kosteli A, Sugaru E, Haemmerle G, Martin JF, Lei J, Zechner R, Ferrante AW. 2010. Weight loss and lipolysis promote a dynamic immune response in murine adipose tissue. *J Clin Invest* **120**:3466–3479. doi:10.1172/JCI42845

Le Ray D, Barry JD, Easton C, Vickerman K. 1977. First tsetse fly transmission of the "AnTat" seroderme of Trypanosoma brucei. *Ann Soc Belg Med Trop* **57**.

Machado H, Bizarra-Rebelo T, Costa-Sequeira M, Trindade S, Carvalho T, Rijo-Ferreira F, Pacheco BR, Serre K, Figueiredo LM. 2021. Trypanosoma brucei triggers a broad immune response in the adipose tissue. *PLoS Pathog* **17**:e1009933. doi:10.1371/JOURNAL.PPAT.1009933

Magez S, Radwanska M, Beschin A, Sekikawa K, de Baetselier P. 1999. Tumor Necrosis Factor Alpha Is a Key Mediator in the Regulation of Experimental Trypanosoma brucei Infections. *Infect Immun* **67**:3128. doi:10.1128/IAI.67.6.3128-3132.1999

Malvy D, Chappuis F. 2011. Sleeping sickness. *Clin Microbiol Infect* **17**:986–995. doi:10.1111/J.1469-0691.2011.03536.X

Mou Z, Jia P, Kuriakose S, Khadem F, Uzonna JE. 2010. Interleukin-17-Mediated Control of Parasitemia in Experimental Trypanosoma congolense Infection in Mice. *Infect Immun* **78**:5271. doi:10.1128/IAI.00168-10

Nogueira G, Solon C, Carraro RS, Engel DF, Ramalho AF, Sidarta-Oliveira D, Gaspar RS, Bombassaro B, Vasques AC, Geloneze B, Vinolo MA, Donato Junior J, Velloso LA. 2020. Interleukin-17 acts in the hypothalamus reducing food intake. *Brain Behav Immun* **87**:272–285. doi:10.1016/J.BBI.2019.12.012

Raheem KA. 2014. A Review of Trypanosomosis-Induced Reproductive Dysfunctions in Male Animals. *Agrosearch* **14**:30–38. doi:10.4314/agrosh.v14i1.4

Schindelin J, Arganda-Carreras I, Frise E, Kaynig V, Longair M, Pietzsch T, Preibisch S, Rueden C, Saalfeld S, Schmid B, Tinevez JY, White DJ, Hartenstein V, Eliceiri K, Tomancak P, Cardona A. 2012. Fiji: an open-source platform for biological-image analysis. *Nature Methods 2012 9:7* **9**:676–682. doi:10.1038/nmeth.2019

Shi L, Salamon H, Eugenin EA, Pine R, Cooper A, Gennaro ML. 2015. Infection with Mycobacterium tuberculosis induces the Warburg effect in mouse lungs. *Scientific Reports 2015 5:1* **5**:1–13. doi:10.1038/srep18176

Sun X, Feng X, Wu X, Lu Y, Chen K, Ye Y. 2020. Fat Wasting Is Damaging: Role of Adipose Tissue in Cancer-Associated Cachexia. *Front Cell Dev Biol* **8**:33. doi:10.3389/FCELL.2020.00033/BIBTEX

Trindade S, Rijo-Ferreira F, Carvalho T, Pinto-Neves D, Guegan F, Aresta-Branco F, Bento F, Young SA, Pinto A, van den Abbeele J, Ribeiro RM, Dias S, Smith TK, Figueiredo LM. 2016. Trypanosoma brucei Parasites Occupy and Functionally Adapt to the Adipose Tissue in Mice. *Cell Host Microbe* **19**:837–848. doi:10.1016/j.chom.2016.05.002

Uranga AP, Levine J, Jensen M. 2005. Isotope tracer measures of meal fatty acid metabolism: Reproducibility and effects of the menstrual cycle. *Am J Physiol Endocrinol Metab* **288**:547–555. doi:10.1152/AJPENDO.00340.2004/ASSET/IMAGES/LARGE/ZH10030520040007.JPEG

Vale PF, Jardine MD. 2015. Sex-specific behavioural symptoms of viral gut infection and Wolbachia in Drosophila melanogaster. *J Insect Physiol* **82**:28–32. doi:10.1016/J.JINSPHYS.2015.08.005

van Marken Lichtenbelt WD, Schrauwen P. 2011. Implications of nonshivering thermogenesis for energy balance regulation in humans. *Am J Physiol Regul Integr Comp Physiol* **301**:285–296.

doi:10.1152/AJPREGU.00652.2010/ASSET/IMAGES/LARGE/ZH60071176070002.JPEG

Wickham H, Averick M, Bryan J, Chang W, D' L, Mcgowan A, François R, Grolemund G, Hayes A, Henry L, Hester J, Kuhn M, Lin Pedersen T, Miller E, Bache SM, Müller K, Ooms J, Robinson D, Seidel DP, Spinu V, Takahashi K, Vaughan D, Wilke C, Woo K, Yutani H. 2019. Welcome to the Tidyverse. *J Open Source Softw* **4**:1686. doi:10.21105/JOSS.01686

Wu H, Liu G, Shi M. 2017. Interferon Gamma in African Trypanosome Infections: Friends or Foes? *Front Immunol* **8**:1105. doi:10.3389/FIMMU.2017.01105

Xiao Y, Liu D, Cline MA, Gilbert ER. 2020. Chronic stress and adipose tissue in the anorexic state: endocrine and epigenetic mechanisms. *Adipocyte* **9**:472. doi:10.1080/21623945.2020.1803643

Yao T, Deng Z, Gao Y, Sun J, Kong X, Huang Y, He Z, Xu Y, Chang Y, Yu KJ, Findley BG, Berglund ED, Wang RT, Guo H, Chen H, Li X, Kaufman RJ, Yan J, Liu T, Williams KW. 2017. Ire1a in pomc neurons is required for thermogenesis and glycemia. *Diabetes* **66**:663–673. doi:10.2337/DB16-0533/-/DC1

Yoneshiro T, Kataoka N, Walejko JM, Ikeda K, Brown Z, Yoneshiro M, Crown SB, Osawa T, Sakai J, McGarrah RW, White PJ, Nakamura K, Kajimura S. 2021. Metabolic flexibility via mitochondrial bcaa carrier slc25a44 is required for optimal fever. *Elife* **10**. doi:10.7554/ELIFE.66865

Zhang W, Cline MA, Gilbert ER. 2014. Hypothalamus-adipose tissue crosstalk: neuropeptide Y and the regulation of energy metabolism. *Nutr Metab (Lond)* **11**:27. doi:10.1186/1743-7075-11-27

Zhou X, Johnson JS, Spakowicz D, Zhou W, Zhou Y, Sodergren E, Snyder M, Weinstock GM. 2020. Longitudinal Analysis of Serum Cytokine Levels and Gut Microbial Abundance Links IL-17/IL-22 With Clostridia and Insulin Sensitivity in Humans. *Diabetes* **69**:1833. doi:10.2337/DB19-0592

Zúñiga LA, Shen W-J, Joyce-Shaikh B, Pyatnova EA, Richards AG, Thom C, Andrade SM, Cua DJ, Kraemer FB, Butcher EC. 2010. IL-17 Regulates Adipogenesis, Glucose Homeostasis, and Obesity. *J Immunol* **185**:6947. doi:10.4049/JIMMUNOL.1001269

Figure 1

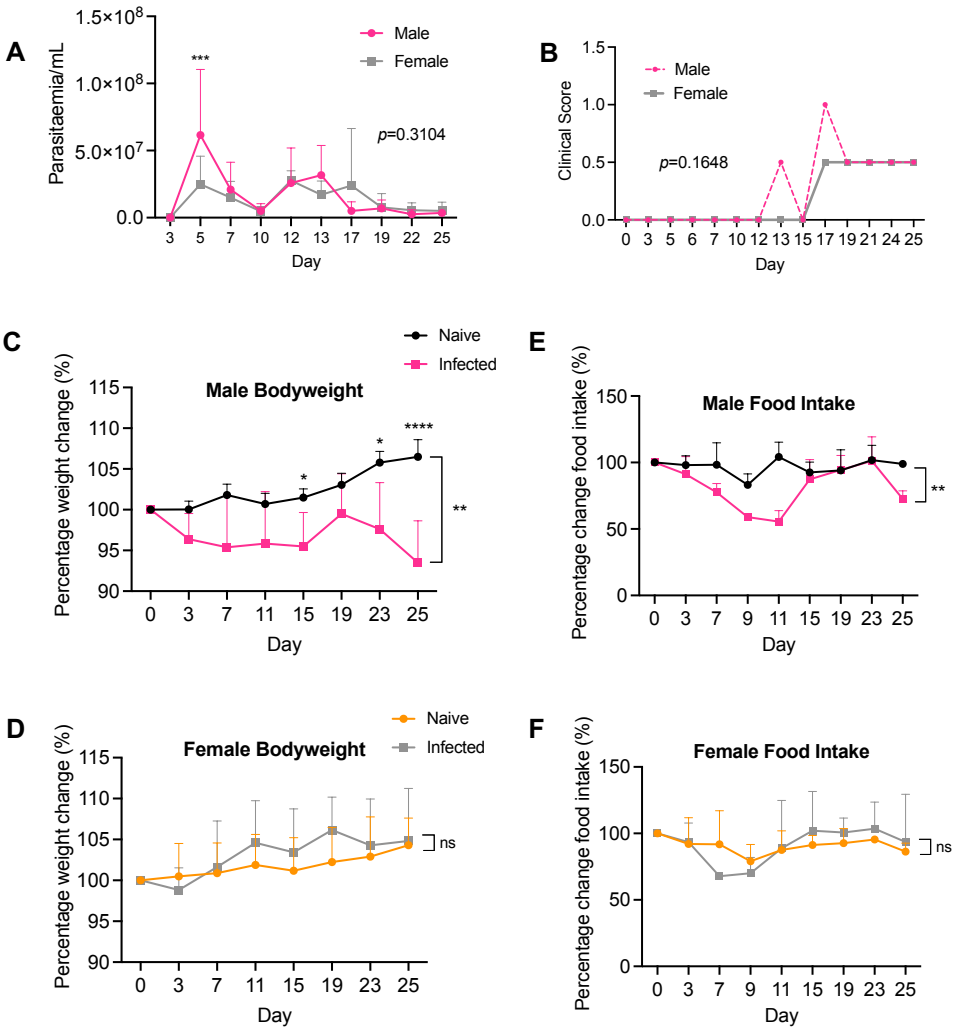

993

Figure 2

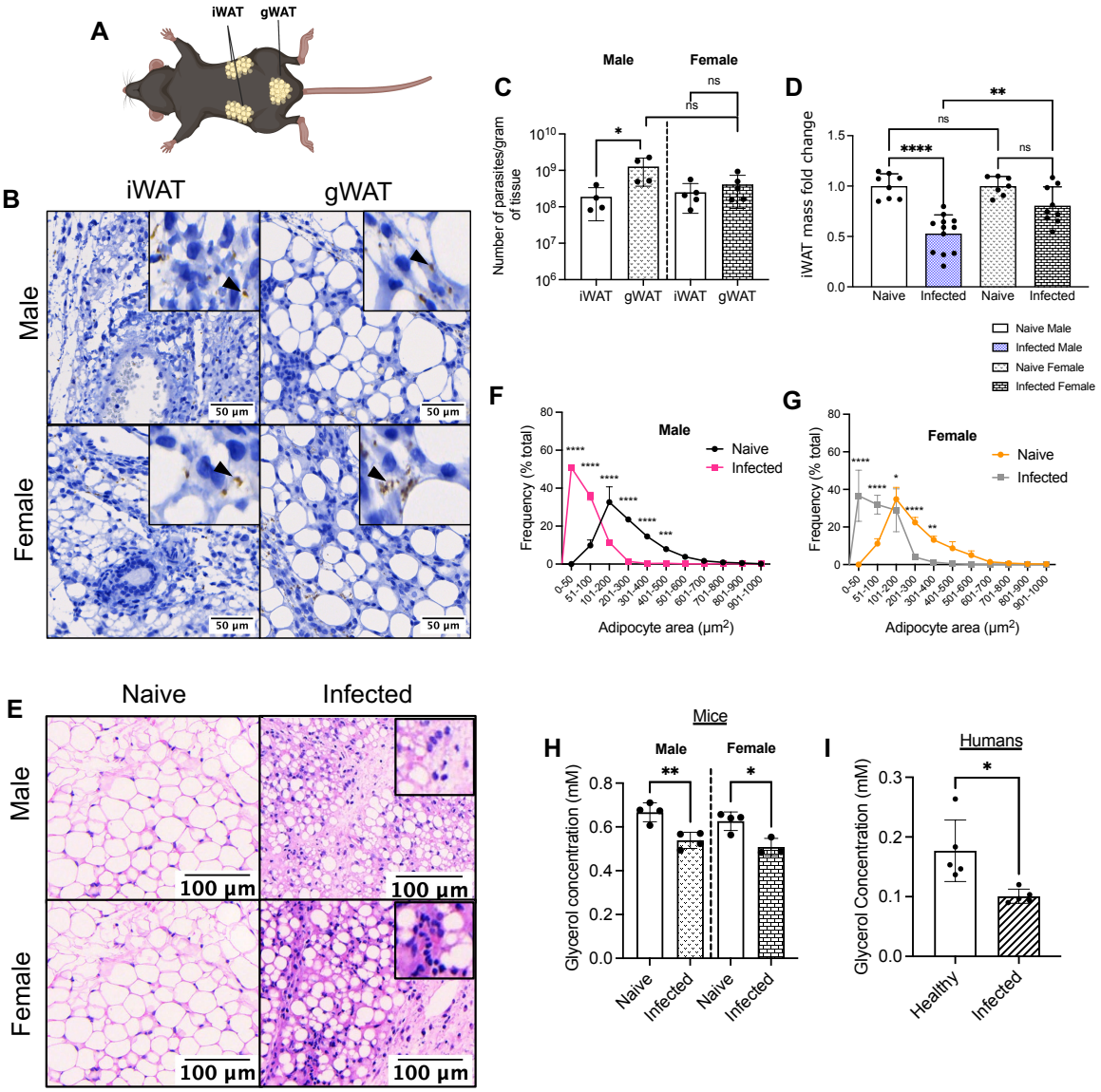

994

Figure 3

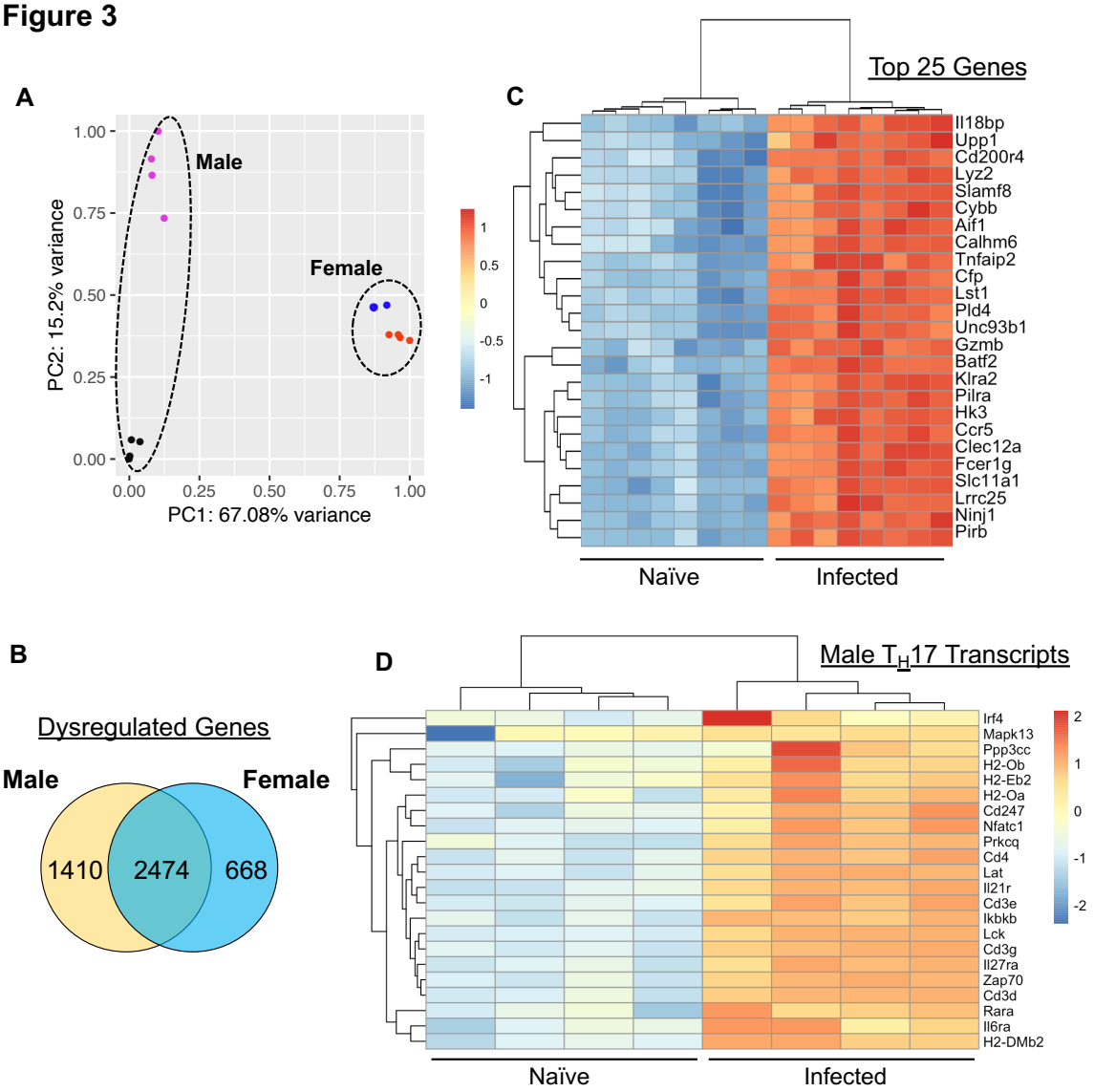
A
Male
Female
PC2: 15.2% variance
PC1: 67.08% variance
1.00
0.75
0.50
0.25
0.00
0.00
0.25
0.50
0.75
1.00
C
Top 25 Genes
Il18bp
Upp1
Cd200r4
Lyz2
Slamf8
Cybb
Aif1
Calhm6
Tnfaip2
Cfp
Lst1
Pld4
Unc93b1
Gzmb
Batf2
Klra2
Pilra
Hk3
Ccr5
Clec12a
Fcer1g
Slc11a1
Lrrc25
Ninj1
Pirb
1
0.5
0
-0.5
-1
Naïve
Infected
B
Dysregulated Genes
Male
Female
1410
2474
668
D
Male T$_H$17 Transcripts
Irf4
Mapk13
Ppp3cc
H2-Ob
H2-Eb2
H2-Oa
Cd247
Nfatc1
Prkcq
Cd4
Lat
Il21r
Cd3e
Ikbkb
Lck
Cd3g
Il27ra
Zap70
Cd3d
Rara
Il6ra
H2-DMb2
2
1
0
-1
-2
Naïve
Infected

995

Figure 4

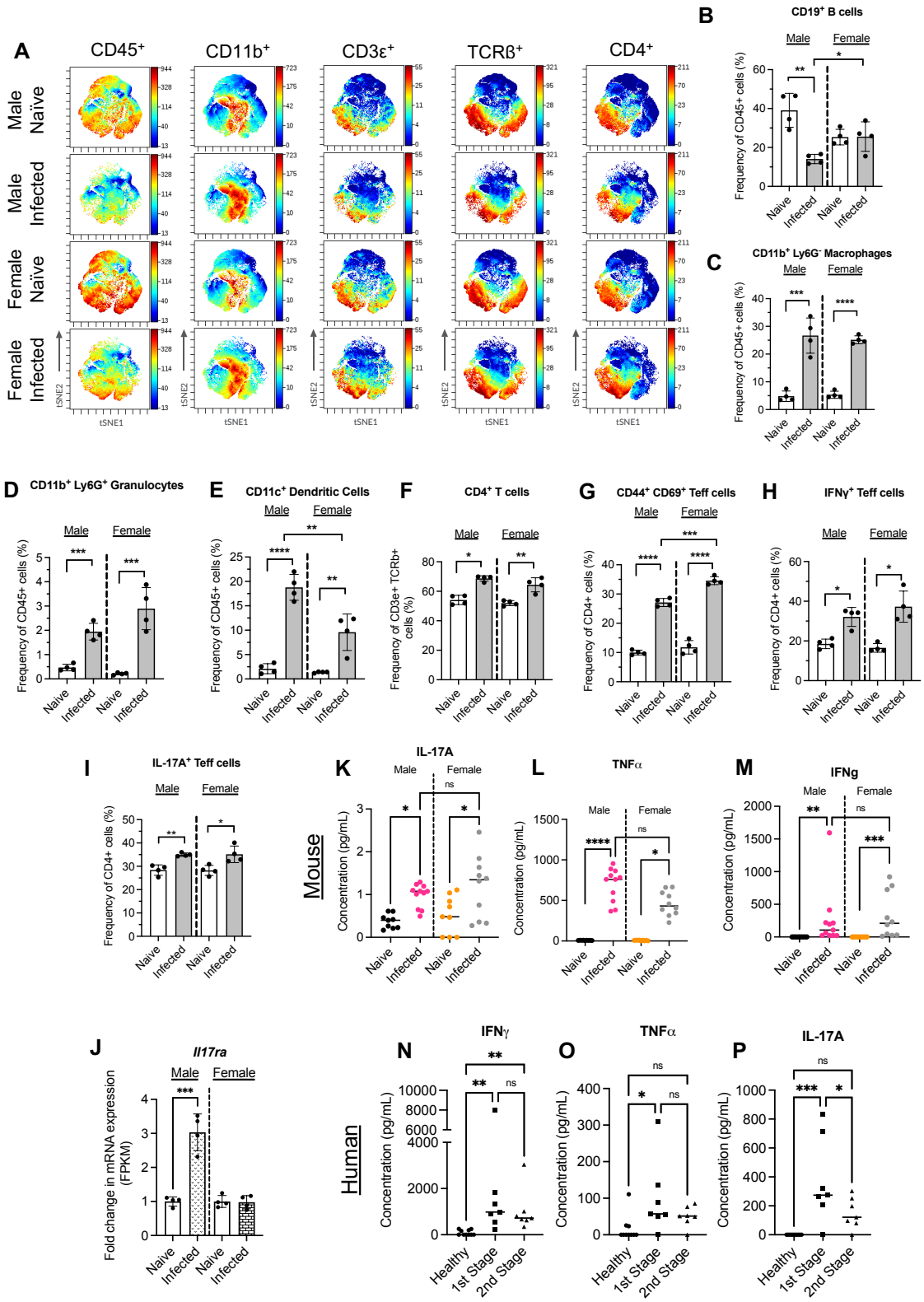
A
CD45+
CD11b+
CD3ε+
TCRß+
CD4+
Male Naive
Male Infected
Female Naive
Female Infected
tSNE1
tSNE2
B
CD19+ B cells
Male
Female
Frequency of CD45+ cells (%)
Naive
Infected
C
CD11b+ Ly6G- Macrophages
D
CD11b+ Ly6G+ Granulocytes
E
CD11c+ Dendritic Cells
F
CD4+ T cells
Frequency of CD3e+ TCRb+ cells (%)
G
CD44+ CD69+ Teff cells
Frequency of CD4+ cells (%)
H
IFNγ+ Teff cells
I
IL-17A+ Teff cells
J
Il17ra
Fold change in mRNA expression (FPKM)
K
IL-17A
Mouse
Concentration (pg/mL)
L
TNFα
M
IFNg
N
IFNγ
Human
Healthy
1st Stage
2nd Stage
O
TNFα
P
IL-17A

Figure 5

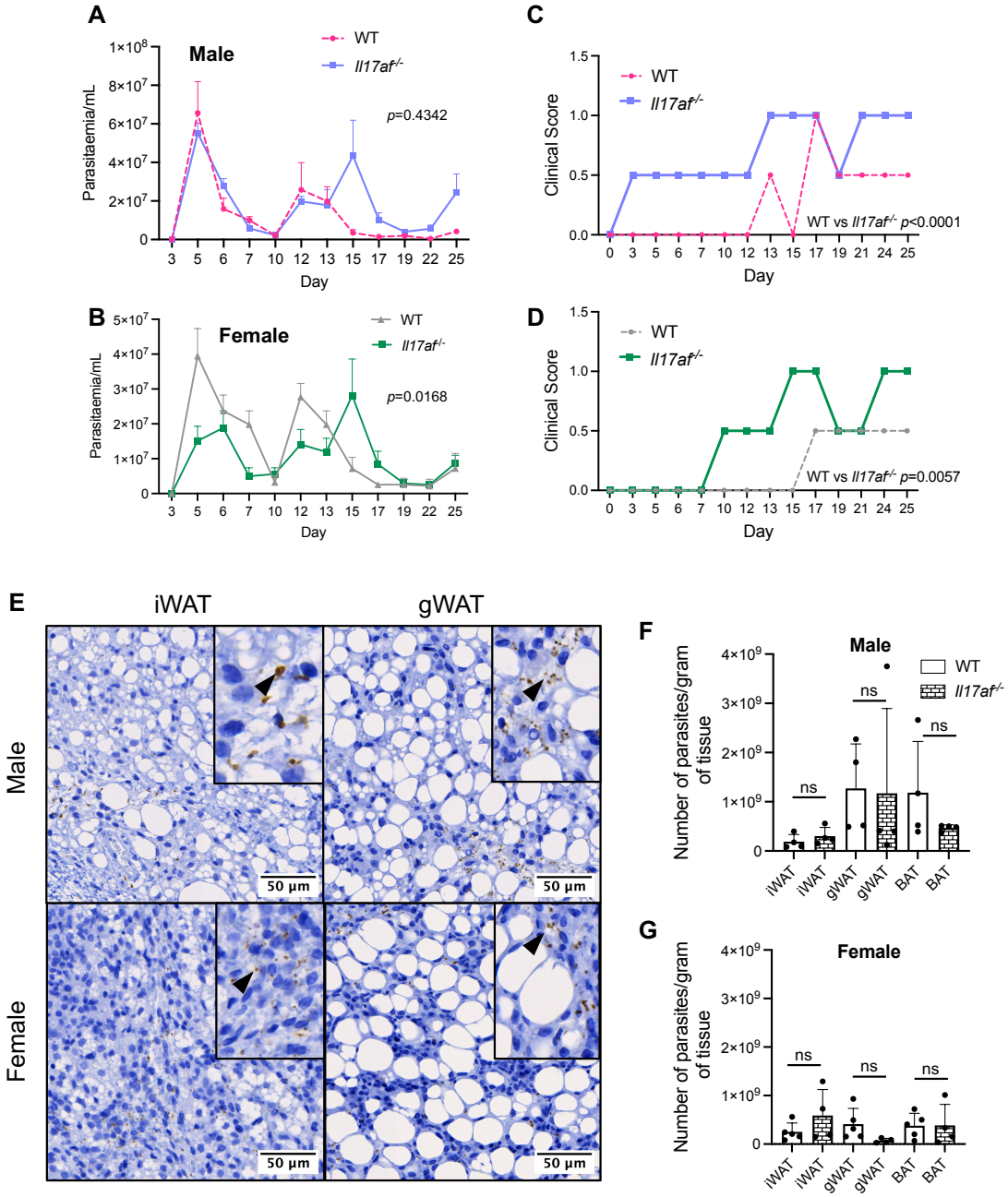
A
Male
WT
Il17af-/-
p=0.4342
Parasitaemia/mL
Day
B
Female
p=0.0168
C
Clinical Score
WT vs Il17af-/- p<0.0001
D
WT vs Il17af-/- p=0.0057
E
iWAT
gWAT
Male
Female
50 µm
F
Male
Number of parasites/gram of tissue
ns
iWAT
gWAT
BAT
G
Female

997

Figure 6

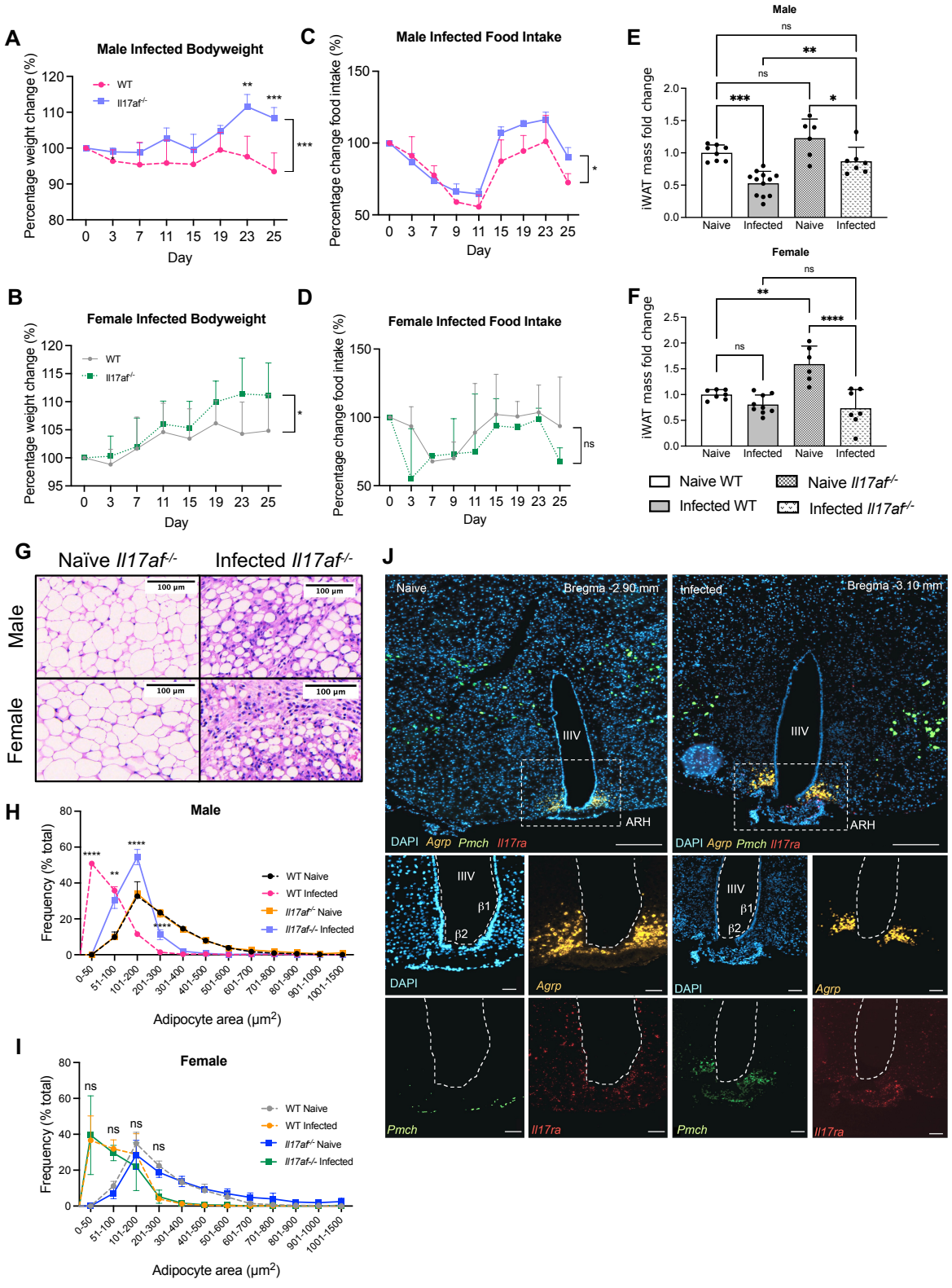

998

999